Mathematical Biosciences and Engineering

MBE, 18(5): 6066–6078.
DOI: 10.3934/mbe.2021303
Received: 26 May 2021
Accepted: 05 July 2021
Published: 07 July 2021

http://www.aimspress.com/journal/MBE

Research article

Brain network analyses of diffusion tensor imaging for brain aging

Song Xu[1,3], Xufeng Yao[1,2,3,*], Liting Han[1,3], Yuting Lv[1,3], Xixi Bu[1,3], Gan Huang[1,3], Yifeng Fan[4], Tonggang Yu[5] and Gang Huang[1,2,3]

[1] College of Medical Imaging, Shanghai University of Medicine and Health Sciences, Shanghai 201318, China
[2] Shanghai Key Laboratory of Molecular Imaging, Shanghai University of Medicine and Health Sciences, Shanghai 201318, China
[3] School of Medical Instrument and Food Engineering, University of Shanghai for Science and Technology, Shanghai 200093, China
[4] School of Medical Imaging, Hangzhou Medical College, Hangzhou 310053, China
[5] Shanghai Gamma Knife Hospital, Fudan University, Shanghai 200235, China

* **Correspondence:** Email: yao6636329@hotmail.com.

Abstract: The approach of graph-based diffusion tensor imaging (DTI) networks has been used to explore the complicated structural connectivity of brain aging. In this study, the changes of DTI networks of brain aging were quantitatively and qualitatively investigated by comparing the characteristics of brain network. A cohort of 60 volunteers was enrolled and equally divided into young adults (YA) and older adults (OA) groups. The network characteristics of critical nodes, path length (L_p), clustering coefficient (C_p), global efficiency (E_{global}), local efficiency (E_{local}), strength (S_p), and small world attribute (σ) were employed to evaluate the DTI networks at the levels of whole brain, bilateral hemispheres and critical brain regions. The correlations between each network characteristic and age were predicted, respectively. Our findings suggested that the DTI networks produced significant changes in network configurations at the critical nodes and node edges for the YA and OA groups. The analysis of whole brains network revealed that L_p, C_p increased ($p < 0.05$, positive correlation), E_{global}, E_{local}, S_p decreased ($p < 0.05$, negative correlation), and σ unchanged ($p \geq 0.05$, non-correlation) between the YA and OA groups. The analyses of bilateral hemispheres and brain regions showed similar results as that of the whole-brain analysis. Therefore the proposed scheme of DTI networks could be used to evaluate the WM changes of brain aging, and the network characteristics of critical nodes exhibited valuable indications for WM degeneration.

Keywords: brain aging; diffusion tensor imaging (DTI); network characteristics; white matter (WM); critical nodes

1. Introduction

Brain aging is mainly characterized by cognitive decline during the normal neurodegenerative process [1]. It has caused serious social burdens and aroused widespread concern. The magnetic resonance imaging (MRI) neuroimaging is a promising technique to investigate the neural basis of cognitive impairments. Different from conventional MRI, diffusion tensor imaging (DTI) could reflect non-random motion of water molecules in a variety of diffusion measures [2] and even noninvasively reconstruct white matter (WM) fiber tracts in the human brain *in vivo* [3,4]. It has become a novel imaging modality for evaluating brain WM [5,6]. Especially, the tract characteristics derived from DTI have been widely used in clinical to study brain development and neurological diseases [7–10].

In general, DTI WM tract characteristics were divided into three types: geometry, diffusion, and networks or connectomes. The geometry characteristics of WM tracts, including fiber length, tract volume, and fiber number, describe the morphological properties of reconstructed fiber tracts [11,12]. While diffusion characteristics of WM tracts represent the water diffusion properties of neural fibers with the metrics of fractional anisotropy (FA), apparent diffusion coefficient (ADC), radial diffusivity (RD) [13–16]. Besides, the deduced DTI network characteristics have been used to describe the changes of DTI brain networks, and have become a hot spot of brain research [17].

Complex network analyses originated from graph theory have been proved to be able to reliably quantify brain functional and structural networks with certain neurobiologically measures [18]. The information about of the DTI structural networks could promote the understanding of brain abnormal development, traumatic brain injury, and neurodegenerative diseases [19]. Also, the performance of DTI networks was validated, and the investigation of DTI network characteristics demonstrated reasonable explanations for the evaluation of binary and weighted DTI networks [20].

A series of neuroscientific investigations have recently identified age-related abnormalities in brain networks. In the literature, a preliminary study revealed that the four DTI network efficiency measures, i.e., native global efficiency (E_{native}), normalized global efficiency (E_{norm}), integrated global efficiency (E_{int}) and local efficiency (E_{loc}), were negatively correlated with age, and these network measures showed the same decreased trend with brain aging [21]. The network-based statistical analysis found that there existed disrupted WM structural connectivity between significant brain regions for young-old and middle-aged groups during the brain aging process [22]. Moreover, the global DTI network properties, such as network strength, cost, topological efficiency, and robustness, followed an inverted U-shaped trajectory with a peak age around the third decade, and different brain regions had heterogeneous trajectories across the human lifespan [23]. According to the hub nodes of brain connectivity, it showed close correlation with the anatomy of brain disorders, and the highly connected hub nodes were considered functionally valuable because their topological centrality supported integrative processing and adaptive behavior [24]. In addition, two major approaches, hub measurement and vulnerability measurement had been used to detect critical nodes within brain networks and to determine the relationships between the identified critical nodes of DTI networks [25]. Generally, the previous studies of brain aging via DTI networks showed varied

reliabilities and capabilities. However, the above approaches didn't fully consider the complicated changes of DTI networks during brain aging. Moreover, the consistency of results still need to be detailedly addressed due to the lack of gold standard data set as well as the implemented approaches.

In our study, one improved scheme of DTI brain networks was proposed and the DTI brain networks were quantitatively and qualitatively evaluated for the two groups of young adults (YA) and old adults (OA). The novelties of our method was summarized as follows: 1) The analyses of DTI brain networks were given for a comprehensive evaluation at the three aspects of critical nodes, node edges and network characteristics for the YA and OA groups, especially for the analyses of network characteristics across the three levels of the whole brain, bilateral hemispheres and critical brain regions; 2) The correlations between each network characteristic and age were further predicted, respectively. Here, the network characteristics of path lengths (L_p), clustering coefficient (C_p), global efficiency (E_{global}), local efficiency (E_{local}), strength (S_p), and small world attribute (σ) were measured. This would provide insights into the normal WM aging of the human brain.

2. Materials and methods

2.1. Materials

The retrospective study has complied with the standard guidelines of our local ethics committee. With permission, the requirement for written informed consent was waived. With the announcement of eligibility criteria in public, the potential participants were recruited for participating in the cohort study. The enrolled criteria were listed as follows: 1) right-handedness; 2) no symptoms or signs of any neurological diseases; 3) no history of craniocerebral surgery or trauma, hypertension, or heart disease; 4) no contraindications to MRI examination, such as the implantation of a pacemaker, non-removable denture and other metal implants in the body; 5) no impairment of brain; 6) no brain lesions verified by MRI scans. Moreover, the classification of young and old by age according to the World Health Organization and the National Bureau of Statistics of China was referenced [26]. And, the samples were verified for normal distributions and variance homogeneities or not. If not, the abnormal sample would be excluded from our study. A total of 60 healthy adults was ultimately included and divided into two groups of YA (14 men and 16 women; age range, 21–30 years; median age, 23 years) and OA (12 men and 18 women; age range, 60–72 years; median age, 64 years) and the demographics of the subjects are listed in Table 1.

Table 1. Characteristics of the subjects (mean ± SD).

Groups	YA	OA	p
No. of Subjects	30	30	—
Sex (female/male)	14/16	12/18	0.604
Age (year)	26.20 ± 6.94	64.27 ± 3.02	0.000*****
Education (year)	16.43 ± 0.46	15.27 ± 3.89	0.635

* $p < 0.05$.

2.2. MR scans

All MRIs included 3D fat-suppressed post-contrast T1-weighted volumetric isotropic turbo

spin-echo (SE) and DTI acquisitions were performed using a 1.5 T GE Signa MR system (Department of Radiology, Shanghai Gamma Knife Hospital, Fudan University, Shanghai, China), with a standard 6-channel head coil. The imaging parameters of conventional SE sequence were mainly listed as follows: axial T1-weighted imaging (repetition time (TR)/echo time (TE) = 880 / 7.864 msec; field of view (FOV) = 240 × 240 mm^2; matrix size = 224 × 224; section thickness = 3 mm, number of signal averages = 1, acquisition time = 1 minute 33 seconds. Accordingly, the imaging parameters of DTI sequence were also as follows: TR/TE = 10000/116.9 msec; b factors = 1000 s/mm^2; diffusion gradient = 15; section thickness = 3 mm with no gaps; FOV = 240 × 240 mm^2; matrix = 128 × 128, number of signal averages = 1, acquisition time per direction = 1 minute 34 seconds. The transverse views were acquired for all scans.

2.3. DTI network construction

The construction of DTI network pipeline was composed by three steps: data prepossessing, deterministic tractography and network construction. And it was performed using PANDA software (v.1.3.1; State Key Laboratory of Cognitive Neuroscience and Learning, Beijing Normal University, Beijing, China, https: //www.nitrc.org/projects/panda/) [27].

2.3.1. Prepossessing

The data was prepossessed via data format conversion, sampling resolution, skull removal, cropping gap, local diffusion homogeneity, normalization, smoothing, and eddy current correction [28–30].

2.3.2. Tracking of WM fibers

The algorithm of fiber assignment by continuous tracking (FACT) was used to reconstruct WM tracts of the whole brain. The fiber tracking was initially tracked from the defined seed points along dual orientations with a fixable step size [31]. The termination criteria were as follows: the threshold of tracking angle was 45°, the threshold of FA was 0.2, and the interpolation was spline filter [32].

2.3.3. Construction of DTI network

In our experiment, undirected weighted DTI networks were constructed by defined nodes and node edges. Here, the nodes represent the corresponding brain regions and the node edges stand for the connections between two neighboring brain regions. The pipeline of network construction consisted of: 1) with the WM labeling atlas of rICBM_DTI, the individual T1 weighted images were co-registered to the space of the Montreal Neurological Institute (MNI); 2) the automated anatomical labeling (AAL) atlas of MNI space was inversely transformed to the standard space; 3) 90 cortical regions parcellated by AAL atlas were defined as brain network nodes [33]; 4) node edges were connected if the number of fibers between nodes was greater than three; 5) each element of the 90 × 90 network connection matrix was computed by multiplying the mean FA by the number of fibers; 6) with the defined nodes, node edges and network connection matrix, DTI network was constructed.

2.4. DTI network characteristics

As usual complex network analysis of graph theory, six network characteristics of L_p, C_p, E_{global}, E_{local}, S_p and σ were evaluated [34]. Here, the DTI brain network characteristics of critical nodes, L_p, C_p, E_{global}, E_{local}, S_p and σ, were defined as follows [35–38]: 1) critical nodes were selected by nodes with greater than averaged nodal betweenness centrality (BC); 2) L_p represented the shortest path length between nodes; 3) C_p indicated the degree of node clustering; 4) E_{global} quantified the efficiency of parallel information transfer for the whole brain network; 5) E_{local} denoted the mean value of the sums of neighboring sub-networks from $E_{global(i)}$; 6) S_p represented the extent of connectivity of the whole brain network was the averaged sums of edge weights $S_{p(i)}$; 7) σ, small world attribute, reflected the transmission efficiency of brain networks.

2.5. Experimental setup

The DTI network characteristics of L_p, C_p, E_{global}, E_{local}, S_p, and σ were compared across the three levels of the whole brain, bilateral hemispheres, and critical brain regions for YA and OA groups. In our study, the network characteristics were measured at the maximum sparse degree with the threshold of 0.4. If the sparse degree above 0.4, the σ would decrease below 1.1 and the network would lose the attribute of small world [39]. During the brain regions analyses, four network characteristics (L_p, C_p, E_{global}, and E_{local}) of critical nodes were evaluated. Here, the network characteristics of L_p, C_p, E_{global}, E_{local}, S_p, and σ were measured by the software of GRETNA (v.2.0; State Key Laboratory of Cognitive Neuroscience and Learning, Beijing Normal University, Beijing, China, https: //www.nitrc.org/projects/gretna) [40]. The nodes, node edges, and brain networks were visualized by BrainNet Viewer (v.1.7; State Key Laboratory of Cognitive Neuroscience and Learning, Beijing Normal University, Beijing, China, http: //www.nitrc.org/projects/bnv/) [41]. And the critical nodes and whole network configurations were visually inspected by two experienced radiologists.

2.6. Statistical analyses

For all network analysis, the independent sample t-tests were conducted to evaluate the statistical differences of network characteristics between the YA and OA groups, respectively. As the most stringent multiple hypothesis test correction method, the Bonferroni correction was used to control the family wise error rate, a two-tailed probability value of $p < 0.05$ was considered statistically significant. Moreover, the correlations between network characteristics and age were conducted by Pearson correlation. The correlation coefficient of r was used to define the degree of positive or negative correlation across the whole cohort (YA and OA). It was a linear correlation with the scope ranging from -1 to 1. Larger absolute r values indicate stronger correlation and vice versa. Here, 0 is the weakest correlation. The SPSS software (v.19.0; IBM Corp., Armonk, NY, USA) was used for all statistical analyses.

3. Results

3.1. Qualitative evaluation

3.1.1. Comparison of critical nodes in DTI networks

In total, there were 15 critical nodes including 1 critical node of Fusiform gyrus Left (FFG.L) for the YA group, and 1 critical node of Superior temporal gyrus Right (STG.R) for the OA group, 13 common critical nodes of Precuneus Left (PCUN.L), Precuneus Right (PCUN.R), Calcarine fissure and surrounding cortex Left (CAL.L), Calcarine fissure and surrounding cortex Right (CAL.R), Middle temporal gyrus Left (MTG.L), Middle temporal gyrus Right (MTG.R), Median cingulate and paracingulate gyri Left (DCG.L), Median cingulate and paracingulate gyri Right (DCG.R), Anterior cingulate and paracingulate gyri Left (ACG.L), Anterior cingulate and paracingulate gyri Right (ACG.R), Lingual gyrus Left (LING.L), Lingual gyrus Right (LING.R), Fusiform gyrus Right (FFG.R) for the YA and OA groups (Table 2).

Among the 15 critical nodes, 7 nodes (PCUN.R, MTG.L, MTG.R, DCG.R, ACG.L, ACG.R, and FFG.L) become smaller, and another 8 nodes (PCUN.L, CAL.L, CAL.R, DCG.L, LING.L, LING.R, FFG.R, and STG.R) showed no significant changes. The critical nodes were mainly located in the prefrontal and occipital lobes, and part in the temporal lobe (Figure 1).

Table 2. The common and different critical nodes for the YA and OA groups.

Groups	Common critical nodes	Different critical nodes
YA	PCUN.L, PCUN.R, CAL.L, CAL.R, MTG.L, MTG.R, DCG.L,	FFG.L
OA	DCG.R, ACG.L, ACG.R, LING.L, LING.R, FFG.R	STG.R

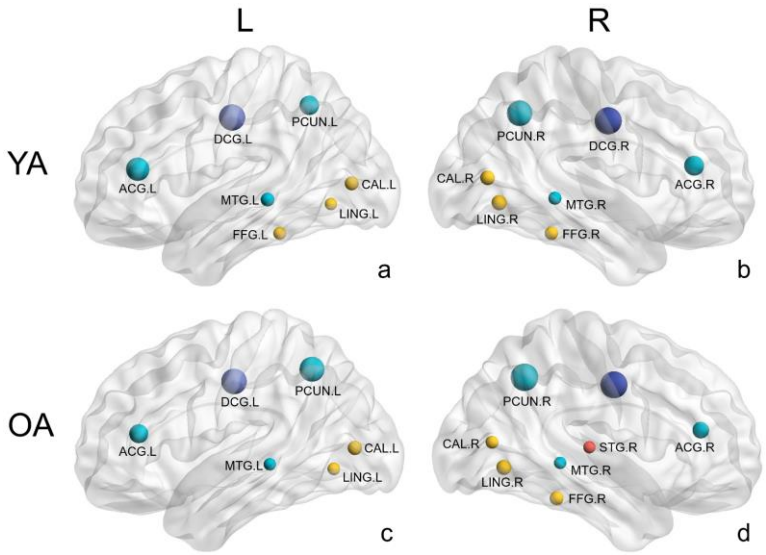

Figure 1. Comparison of critical nodes in DTI networks between the YA and OA groups.

3.1.2. Comparison of node edges in DTI networks

DTI networks of YA and OA groups represented similar node edges in network configurations (Figure 2). Compared to the DTI networks of YA, the DTI networks of OA demonstrated weak connections of node edges at the frontal and occipital lobes, as indicated by blue arrows.

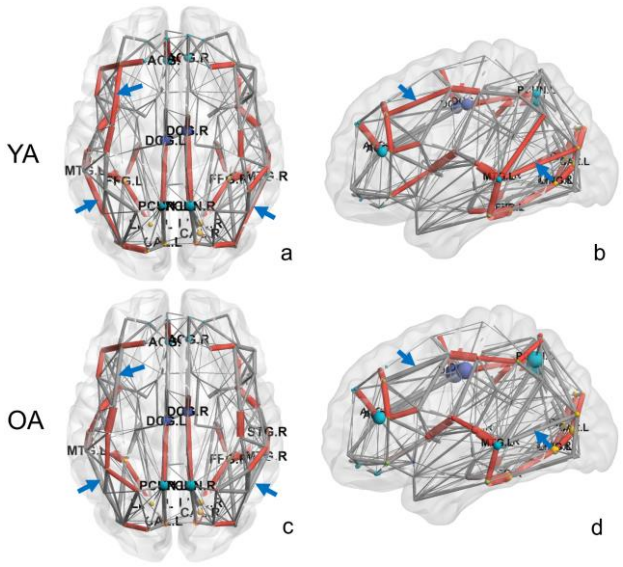

Figure 2. Comparison of node edges in DTI networks between the YA and OA groups. (Red for strong edge connection, gray for weak edge connection.)

3.2. Quantitative evaluation

3.2.1. Comparison of network characteristics of the whole brain

The whole-brain network characteristics measured are listed in Table 3. It showed that the network characteristics of L_p, C_p increased ($p < 0.05$, positive correlation), and E_{global}, E_{local}, S_p decreased ($p < 0.05$, negative correlation). While there were no significant changes of δ between the YA and OA groups ($p \geq 0.05$, non-correlation).

Table 3. Comparison of DTI network characteristics of whole brain between the YA and OA groups.

Groups	L_p	C_p	E_{global}	E_{local}	S_p	σ
YA	0.064 ± 0.009	0.036 ± 0.005	15.831 ± 2.259	28.069 ± 3.855	283.099 ± 41.925	4.165 ± 0.304
OA	0.072 ± 0.011	0.039 ± 0.006	14.187 ± 2.232	25.258 ± 3.933	237.773 ± 37.402	4.066 ± 0.286
p	0.004*	0.036*	0.007*	0.006*	0.017*	0.200
r	0.380*	0.283*	-0.359*	-0.353*	-0.318*	-0.178

*$p < 0.05$, r: Pearson correlation coefficient.

3.2.2. Comparison of network characteristics of bilateral hemispheres

Accordingly, the DTI network characteristics of bilateral hemispheres are listed in Table 4. It was clear that the L_p increased for bilateral hemispheres ($p < 0.05$, positive correlation), E_{global} and E_{local} decreased for bilateral hemispheres ($p < 0.05$, negative correlation), C_p increased for right hemisphere ($p < 0.05$, positive correlation). While there were no significant changes for C_p of the left hemisphere between the YA and OA groups ($p \geq 0.05$, non-correlation).

Table 4. Comparison of DTI network characteristics of bilateral hemispheres between the YA and OA groups.

Groups	Left Hemisphere				Right Hemisphere			
	L_p	C_p	E_{global}	E_{local}	L_p	C_p	E_{global}	E_{local}
YA	0.068 ± 0.010	0.036 ± 0.006	16.000 ± 2.260	28.350 ± 3.930	0.069 ± 0.010	0.035 ± 0.006	15.680 ± 2.290	27.780 ± 4.128
OA	0.080 ± 0.019	0.039 ± 0.007	14.120 ± 2.200	24.980 ± 3.780	0.077 ± 0.013	0.039 ± 0.007	14.250 ± 2.370	25.530 ± 4.433
p	0.001*	0.065	0.002*	0.001*	0.010*	0.040*	0.022*	0.046*
r	0.415*	0.262*	-0.404*	-0.416*	0.336*	0.266*	-0.303*	-0.265*

*p < 0.05, r: Pearson correlation coefficient.

Table 5. Comparison of DTI network characteristics of critical nodes between the YA and OA groups.

Groups	L_p				C_p				E_{global}				E_{local}			
	YA	OA	p	r	YA	OA	p	r	YA	OA	p	r	YA	OA	p	r
ACG.L	0.05 ± 0.01	0.06 ± 0.01	*	*	0.03 ± 0.01	0.03 ± 0.01	-	-	20.01 ± 3.76	16.81 ± 2.93	*	*	18.14 ± 3.83	15.69 ± 3.71	*	*
ACG.R	0.06 ± 0.01	0.06 ± 0.01	*	*	0.03 ± 0.01	0.03 ± 0.01	-	-	18.93 ± 3.46	16.52 ± 3.06	*	*	19.37 ± 4.94	15.54 ± 3.68	*	*
DCG.L	0.05 ± 0.01	0.06 ± 0.01	*	*	0.03 ± 0.01	0.03 ± 0.01	-	-	20.65 ± 3.80	17.74 ± 4.11	*	*	19.61 ± 7.05	15.42 ± 6.41	*	*
DCG.R	0.05 ± 0.01	0.06 ± 0.01	*	*	0.03 ± 0.01	0.02 ± 0.01	-	-	21.26 ± 3.69	18.25 ± 4.16	*	*	21.22 ± 6.10	17.40 ± 5.67	*	*
CAL.L	0.05 ± 0.01	0.06 ± 0.01	*	*	0.03 ± 0.01	0.03 ± 0.01	-	-	18.89 ± 3.08	17.24 ± 3.10	*	*	25.13 ± 5.56	19.46 ± 4.96	*	*
CAL.R	0.05 ± 0.01	0.06 ± 0.01	*	*	0.03 ± 0.01	0.03 ± 0.01	-	-	19.69 ± 3.72	17.62 ± 3.39	*	*	25.83 ± 5.13	23.15 ± 6.73	-	-
LING.L	0.05 ± 0.01	0.06 ± 0.01	*	*	0.03 ± 0.01	0.03 ± 0.01	-	-	18.93 ± 2.76	16.68 ± 2.67	*	*	25.59 ± 5.04	21.65 ± 5.46	*	*
LING.R	0.05 ± 0.01	0.06 ± 0.01	*	*	0.03 ± 0.01	0.04 ± 0.01	-	-	19.14 ± 3.27	17.42 ± 3.36	*	*	26.31 ± 7.07	23.37 ± 5.66	-	-
FFG.R	0.05 ± 0.01	0.05 ± 0.01	*	*	0.04 ± 0.01	0.05 ± 0.01	*	*	21.32 ± 3.40	19.34 ± 3.40	*	*	25.26 ± 7.03	21.80 ± 5.62	*	*
PCUN.L	0.05 ± 0.01	0.06 ± 0.02	*	*	0.03 ± 0.01	0.03 ± 0.01	-	-	19.33 ± 3.42	17.38 ± 3.95	*	*	23.20 ± 4.89	19.73 ± 4.58	*	*
PCUN.R	0.05 ± 0.01	0.06 ± 0.01	*	*	0.02 ± 0.01	0.02 ± 0.01	-	-	20.84 ± 3.59	18.04 ± 4.14	*	*	19.79 ± 4.85	17.53 ± 4.45	-	*
MTG.L	0.05 ± 0.01	0.06 ± 0.01	*	*	0.04 ± 0.01	0.04 ± 0.01	-	-	22.26 ± 3.29	18.77 ± 3.51	*	*	23.95 ± 5.13	22.22 ± 5.20	-	-
MTG.R	0.05 ± 0.01	0.05 ± 0.01	*	*	0.04 ± 0.01	0.04 ± 0.01	-	-	21.51 ± 3.67	19.29 ± 3.41	*	*	24.58 ± 6.98	24.36 ± 6.55	-	-

*p < 0.05, r: Pearson correlation coefficient.

3.2.3. Comparison of network characteristics of brain regions

The network characteristics of the 13 critical nodes are listed in Table 5. It was evident that L_p increased ($p < 0.05$, positive correlation), E_{global} decreased ($p < 0.05$, negative correlation), C_p of FFG.R increased ($p < 0.05$, positive correlation), and E_{local} of ACG.L, ACG.R, DCG.L, DCG.R, CAL.L, LING.L, FFG.R, and PCUN.R decreased ($p < 0.05$, negative correlation); other network characteristics showed no significant differences for the YA and OA groups ($p \geq 0.05$).

4. Discussion

This study investigated the changes of DTI network characteristics across the whole brain, bilateral hemispheres, and specific brain regions for brain aging. Our study found that the brain networks showed distinct changes in network structures and information transmission capabilities.

Our findings revealed that the networks of YA and OA groups had similar configurations except for 15 critical nodes. The changed critical nodes meant that the status of critical nodes could be altered during brain aging. The enlarged critical nodes represented the promotion of network status and vice versa. The analyses of network configuration proved that node edges also changed with brain aging. It could be explained that most microstructural changes of brain networks were observed in the prefrontal and temporal lobes accompanying by significant nonlinear changes for brain aging [23].

The increased L_p, C_p, and decreased E_{global}, E_{local}, S_p across the whole brain demonstrated the decreased efficiency of information exchange and transmission with brain aging. The unchanged parameter σ suggested that the brain networks of YA and OA groups both kept small-world properties. It also meant that the DTI networks of OA still had the capability for information transformation. Similarly, the analyses of bilateral hemispheres showed almost the same trend as the whole brain analyses with the exception of the unchanged C_p of the left hemisphere for the YA and OA groups. It was correlated with the topological asymmetry of bilateral hemispheres, and the left hemisphere preserved more reliable network connectivity than the right hemisphere with brain aging [42]. The correlations between the DTI network characteristics and age were consistent with the comparison of network characteristics between groups. The brain topological structure was obviously damaged and accompanied by the declination in cognitive function.

For critical brain regions, the measured network characteristics showed the same trend with the network analyses of the whole brain and bilateral hemisphere. This phenomenon hinted that some chosen critical nodes had consistent transmission capability [43]. While the increased C_p of FFG.R indicated that the reduction of the long-term fiber connections was obvious during brain aging [44]. During brain aging, the changes of E_{local} of critical nodes, such as ACG.L, ACG.R, DCG.L, DCG.R, CAL.L, LING.L, FFG.R, and PCUN.R, were different. The decrease of E_{local} stands for the reduction in transmission efficiency of local networks.

The properties of network topology had close relations with WM changes. Once a previous study demonstrated that the loss of fiber connections between brain regions would lead to the decreased functional connectivity [45,46]. Brain aging was closely related to the disruptions of myelin sheaths, and it was assumed to be at least partly associated with WM degeneration [47]. The damage to neural axons would lead to the consequent decrease in FA. Moreover, the fiber tracts not only become shorter in average length but also reduced fiber number with brain aging [48].

According to the construction of DTI networks, the statuses of critical nodes and node edges eventually changed during brain aging.

Although this study has produced some useful findings, there are still two main limitations to be improved in the future. Firstly, there is no uniform standard for data acquisition and the processing of network construction. Especially, the fast and multiple directions of DTI acquisition are greatly affected by MR equipment, scanning protocols and post-processing approaches. Thus, the reliability or consistency for the DTI network analyses of brain aging needs to be verified by more experiments on a variety of MR scanners. The comparison of different approaches would be further conducted for more convincing results. Secondly, multiple modalities of brain networks should be considered to detect the network changes of brain aging. This would enhance our understanding of brain aging.

5. Conclusions

This work stated that DTI brain networks can be effectively used to evaluate WM changes in the human brain, and the chosen network characteristics provide valuable indications for WM degeneration. For brain aging, the efficiency of the overall brain network information transmission decreases and it accompanies by different trends for specific brain regions.

Acknowledgments

This project was funded by the National Natural Science Foundation of China (Nos. 61971275 and 81830052).

Conflict of interest

We declare that we have no financial and personal relationships with other people or organizations that can inappropriately influence our work, there is no professional or other personal interest of any nature or kind in any product, service and/or company that could be construed as influencing the position presented in, or the review of, the manuscript entitled (Uda et al., 2015).

References

1. O. Carmichael, S. Lockhart, The role of diffusion tensor imaging in the study of cognitive aging, *Curr. Top. Behav. Neurosci.*, **11** (2012), 289–320.
2. A. Qiu, S. Mori, M. I. Miller, Diffusion tensor imaging for understanding brain development in early life, *Annu. Rev. Psychol.*, **66** (2015), 853–876.
3. S. Uda, M. Matsui, C. Tanaka, A. Uematsu, K. Miura, I. Kawana, et al., Normal development of human brain white matter from infancy to early adulthood: a diffusion tensor imaging study, *Dev. Neurosci.*, **37** (2015), 182–194.
4. S. Pujol, W. Wells, C. Pierpaoli, C. Brun, J. Gee, G. Cheng, et al., The DTI challenge: toward standardized evaluation of diffusion tensor imaging tractography for neurosurgery, *J. Neuroimaging*, **25** (2015), 875–882.

5. B. D. Le, J. F. Mangin, C. Poupon, C. A. Clark, S. Pappata, N, Molko, et al., Diffusion tensor imaging: concepts and applications, *J. Magn. Reson. Imaging: Off. J. Int. Society Magn. Reson. Med.*, **13** (2001), 534–546.
6. R. Xue, P. C. M. van Zijl, B. J. Crain, M. Solaiyappan, S. Mori, In vivo three-dimensional reconstruction of rat brain axonal projections by diffusion tensor imaging, *Magn. Reson. Med.: Off. J. Int. Soc. Magn. Reson. Med.*, **42** (1999), 1123–1127.
7. L. Bonilha, E. Gleichgerrcht, J. Fridriksson, C. Rorden, J. L. Breedlove, T. Nesland, et al., Reproducibility of the structural brain connectome derived from diffusion tensor imaging, *PLoS One*, **10** (2015), e0135247.
8. A. L. Alexander, J. E. Lee, M. Lazar, A. S. Field, Diffusion tensor imaging of the brain, *Neurotherapeutics*, **4** (2007), 316–329.
9. P. C. Sundgren, Q. Dong, D. Gomez-Hassan, S. K. Mukherji, P. Maly, R. Welsh, Diffusion tensor imaging of the brain: review of clinical applications, *Neuroradiology*, **46** (2004), 339–350.
10. C. Yan, G. Gong, J. Wang, D. Wang, D. Liu, C. Zhu, et al., Sex-and brain size-related small-world structural cortical networks in young adults: a DTI tractography study, *Cereb. Cortex*, **21** (2011), 449–458.
11. S. H. Jang, S. H. Cho, M. C. Chang, Age-related degeneration of the fornix in the human brain: a diffusion tensor imaging study, *Int. J. Neurosci.*, **121** (2011), 94–100.
12. S. H. Jang, Y. H. Kwon, M. Y. Lee, J. R. Kim, J. P. Seo, Aging of the cingulum in the human brain: Preliminary study of a diffusion tensor imaging study, *Neurosci. Lett.*, **610** (2016), 213–217.
13. O. Abe, H. Yamasue, S. Aoki, M. Suga, H. Yamada, K. Kasai, et al., Aging in the CNS: comparison of gray/white matter volume and diffusion tensor data, *Neurobiol. Aging*, **29** (2008), 102–116.
14. H. Liu, L. Wang, Z. Geng, Q. Zhu, Z. Song, R. Chang, et al., A voxel-based morphometric study of age-and sex-related changes in white matter volume in the normal aging brain, *Neuropsychiatr. Dis. Treat.*, **12** (2016), 453.
15. N. Malykhin, S. Vahidy, S. Michielse, N. Coupland, R. Camicioli, P. Seres, et al., Structural organization of the prefrontal white matter pathways in the adult and aging brain measured by diffusion tensor imaging, *Brain Struct. Funct.*, **216** (2011), 417–431.
16. L. Zhou, N. Tian, Z. J. Geng, B. K. Wu, L. Y. Dong, M. R. Wang, Diffusion tensor imaging study of brain precentral gyrus and postcentral gyrus during normal brain aging process, *Brain Behav.*, **10** (2020), e01758.
17. E. Bullmore, O. Sporns, Complex brain networks: graph theoretical analysis of structural and functional systems, *Nat. Rev. Neurosci.*, **10** (2009), 186–198.
18. L. Deuker, E. T. Bullmore, M. Smith, S. Christensen, P. J. Nathan, B. Rockstroh, et al., Reproducibility of graph metrics of human brain functional networks, *Neuroimage*, **47** (2009), 1460–1468.
19. O. Sporns, G. Tononi, R. Kötter, The human connectome: a structural description of the human brain, *PLoS Comput. Biol.*, **1** (2005), e42.
20. H. Cheng, Y. Wang, J. Sheng, W. G. Kronenberger, V. P. Mathews, T. A. Hummer, et al., Characteristics and variability of structural networks derived from diffusion tensor imaging, *Neuroimage*, **61** (2012), 1153–1164.

21. O. Ajilore, M. Lamar, A. Kumar, Association of brain network efficiency with aging, depression, and cognition, *Am. J. Geriatr. Psychiatry*, **22** (2014), 102–110.
22. L. Lin, M. Tian, Q. Wang, S. Wu, Diffusion tensor tractography reveals disrupted structural connectivity during brain aging, in *Journal of Physics: Conference Series*, **910** (2017), 012042.
23. T. Zhao, M. Cao, H. Niu, Z. Xi-Nian, A. Evans, Y. He, et al., Age-related changes in the topological organization of the white matter structural connectome across the human lifespan, *Hum. Brain Mapp.*, **36** (2015), 3777–3792.
24. N. A. Crossley, A. Mechelli, J. Scott, F. Carletti, P. T. Fox, P. McGuire, et al., The hubs of the human connectome are generally implicated in the anatomy of brain disorders, *Brain*, **137** (2014), 2382–2395.
25. C. Jin, L. Lin, L. W. Kuo, S. Wu, Z. Fu,Y. P. Chao, The relationships between the identified critical nodes within DTI-based brain structural network using hub measurements and vulnerability measurement, in *2015 37th Annual International Conference of the IEEE Engineering in Medicine and Biology Society (EMBC), IEEE*, (2015), 422–425.
26. W. Wen, R. Luo, X. Tang, L. Tang, H. X. Huang, X. Wen, et, al. Age-related progression of arterial stiffness and its elevated positive association with blood pressure in healthy people, *Atherosclerosis*, **238** (2015), 147–152.
27. Z. Cui, S. Zhong, P. Xu, Y. He, G. Gong, PANDA: a pipeline toolbox for analyzing brain diffusion images, *Front. Hum. Neurosci.*, **7** (2013), 42.
28. G. Gong, Local diffusion homogeneity (LDH): an inter-voxel diffusion MRI metric for assessing inter-subject white matter variability, *PLoS One*, **8** (2013), e66366.
29. W. Chau, A. R. McIntosh, The Talairach coordinate of a point in the MNI space: how to interpret it, *Neuroimage*, **25** (2005), 408–416.
30. J. Ashburner, SPM: a history, *Neuroimage*, **62** (2012), 791–800.
31. J. Klein, A. Grötsch, D. Betz, S. Barbieri, O. Friman, B. Stieltjes, et al., Qualitative and quantitative analysis of probabilistic and deterministic fiber tracking, in *Medical Imaging 2010: Image Processing. International Society for Optics and Photonics*, **7623** (2010), 76232A.
32. S. Mori, Imaging cortical association using diffusion-tensor-based tracts in the human brain axonal tracking, *Magn. Reson. Med.*, **47** (2002), 215–223.
33. N. Tzourio-Mazoyer, B. Landeau, D. Papathanassiou, F. Crivello, O. Etard, N. Delcroix, et al., Automated anatomical labeling of activations in SPM using a macroscopic anatomical parcellation of the MNI MRI single-subject brain, *Neuroimage*, **15** (2002), 273–289.
34. M. Rubinov, O. Sporns, Complex network measures of brain connectivity: uses and interpretations, *Neuroimage*, **52** (2010), 1059–1069.
35. A. Zalesky, A. Fornito, I. H. Harding, L. Cocchi, M. Yücel, C. Pantelis, et al., Whole-brain anatomical networks: does the choice of nodes matter, *Neuroimage*, **50** (2010), 970–983.
36. A. Mantrach, L. Yen, J. Callut, K. Francoisse, M. Shimbo, M. Saerens, The sum-over-paths covariance kernel: A novel covariance measure between nodes of a directed graph, *IEEE Trans. Pattern Anal. Mach. Intell.*, **32** (2009), 1112–1126.
37. F. U. Fischer, D. Wolf, A. Scheurich, A. Fellgiebel, Association of structural global brain network properties with intelligence in normal aging, *PLoS One*, **9** (2014), e86258.
38. Y. Sun, R. Lee, Y. Chen, S. Collinson, N. Thakor, A. Bezerianos, et al., Progressive gender differences of structural brain networks in healthy adults: a longitudinal, diffusion tensor imaging study, *PLoS One*, **10** (2015), e0118857.

39. Y. F. Wang, P. Gu, J. Zhang, R. Qi, M. Veer, G. Zheng, et al. Deteriorated functional and structural brain networks and normally appearing functional-structural coupling in diabetic kidney disease: a graph theory-based magnetic resonance imaging study, *Eur. Radiol.*, **29** (2019), 5577–5589.
40. J. Wang, X. Wang, M. Xia, X. Liao, A. Evans, Y. He, GRETNA: a graph theoretical network analysis toolbox for imaging connectomics, *Front. Hum. Neurosci.*, **9** (2015), 386.
41. M. Xia, J. Wang, Y. He, BrainNet Viewer: a network visualization tool for human brain connectomics, *PLoS One*, **8** (2013), e68910.
42. B. J. Cherry, M. Adamson, A. Duclos, J. B. Hellige, Aging and individual variation in interhemispheric collaboration and hemispheric asymmetry, *Aging neuropsychol. C.*, **12** (2005), 316–339.
43. K. Wu, Y. Taki, K. Sato, H. Qi, R. Kawashima, H. Fukuda, A longitudinal study of structural brain network changes with normal aging, *Front. Hum. Neurosci.*, **7** (2013), 113.
44. Y. Liu, C. Yu, X. Zhang, J. Liu, Y. Duan, A. F. Alexander-Bloch, et al., Impaired long distance functional connectivity and weighted network architecture in Alzheimer's disease, *Cereb. Cortex*, **24** (2014), 1422–1435.
45. G. Gong, Y. He, L. Concha, C. Lebel, D. W. Gross, A. C. Evans, et al., Mapping anatomical connectivity patterns of human cerebral cortex using in vivo diffusion tensor imaging tractography, *Cereb. Cortex*, **19** (2009), 524–536.
46. B. M. Tijms, A. M. Wink, W. de Haan, W. M. van der Flier, C. J. Stam, P. Scheltens, et al., Alzheimer's disease: connecting findings from graph theoretical studies of brain networks, *Neurobiol. Aging*, **34** (2013), 2023–2036.
47. S. Xie, Z. Zhang, F. Chang, Y. Wang, Z. Zhang, Z. Zhou, et al., Subcortical white matter changes with normal aging detected by multi-shot high resolution diffusion tensor imaging, *PLoS One*, **11** (2016), e0157533.
48. M. Di Paola, C. Caltagirone, G. Spalletta, What does the corpus callosum tell us about brain changes in the elderly, *Expert Rev. Neurother.*, **11** (2011), 1557–1560.